Atomistic QM/MM simulations of the strength of covalent interfaces in carbon nanotube-polymer composites: Supplementary Material.

Jacek R Gołębiowski*[1, 2], James R Kermode[3], Peter D Haynes[1, 2, 4], and Arash A Mostofi[1, 2, 4]

[1]Department of Materials, Imperial College London, London SW7 2AZ, U.K.
[2]Thomas Young Centre for Theory and Simulation of Materials, Imperial College London, London SW7 2AZ, U.K.
[3]Warwick Centre for Predictive Modelling, School of Engineering, University of Warwick, Coventry, CV4 7AL, United Kingdom
[4]Department of Physics, Imperial College London, London SW7 2AZ, U.K.

April 5, 2020

1 Methodology

The single carbon nanotube pull-out experiments conducted in this study were carried out using molecular dynamics with interatomic interactions computed via the hybrid QM/MM method introduced in the main text. Additional details regarding the flagging mechanism in our QM/MM method and the dispersion correction used for the interatomic forces are given below.

Flagging mechanism The flagging protocol aims to select atoms residing in areas of the energy landscape where the classical description might be inaccurate by comparing atomic energies derived from the force-field with pre-computed thresholds. These energy thresholds are obtained prior to the main pull-out simulation by simulating the initial system in equilibrium for 10 ps while recording per-atom energies. The mean E_{mean} and standard deviation E_{std} of these per-atom energies determine the flagging threshold E_{th} according to

$$E_{\mathrm{th}} = E_{\mathrm{mean}} + aE_{\mathrm{std}} + b, \tag{1}$$

*Corresponding author, email: jacek.golebiowski14@imperial.ac.uk.

where the parameter a is selected to balance accuracy and computational efficiency and the parameter b represents a small offset to ensure numerical stability for atoms with small energy variance. The thresholds are calculated separately for each atom and as a result, the protocol selects particles based on how much its energy is elevated compared to its normal thermal oscillations. The flagging mechanism that we have used has an in-built hysteresis in the sense that there is a lower energy threshold for atoms that were flagged for quantum mechanical treatment at the previous time-step than for atoms that were treated classically in the previous time-step. This approach prevents oscillations in the QM region size and shape which could introduce instabilities. This is achieved by setting $a = 4$ for atoms within a QM region and $a = 6$ for those not in a QM region at a given time-step. The parameter b was fixed at 0.05 eV.

In most simulations, the majority of time-steps did not involve any QM computations and, when QM was necessary, the total number of atoms treated with the higher level theory was usually below 1% of the total number of atoms (7000) at any given time. An example can be seen in Figure S1 which shows the number of QM atoms at each time-step for some representative examples of the pull-out simulations.

Dispersion correction Dispersion contributions were not included in the DFTB Hamiltonian and the QM forces were adjusted post-hoc by including an empirical correction, following the approach discussed by Zhechkov *et al.* [9]. The corrected force on F is given by $F = F_{\mathrm{QM}} + \alpha F_{\mathrm{LJ}}$, where F is the corrected force, F_{QM} is the force from the QM method without any corrections, and F_{LJ} is the Lennard-Jones (LJ) term of the generalised Amber force-field (GAFF) [8] that is used to describe the classical interactions in the non-QM regions of the system. The correction term is computed based on the pairwise LJ interactions in the whole system.

The parameter α was chosen by examining an ensemble of ten different structures each composed of ten 48-monomer long polyethylene chains packed into a bulk using Monte Carlo based sampling as implemented in the MedeA software package [4]. For each structure, two calculations were performed, one where the whole system was simulated with a QM method and the other where only one selected chain was simulated with the QM method and the forces were corrected by the approach presented above. The optimal value of α is 0.2 and was chosen so that the sum of squared difference between the forces on the selected chain from the former and the latter are minimised. Momentum conservation was ensured by adjusting the sum of total forces to zero.

2 Initial composite cell preparation

The initial polymeric slab was composed of fifty 48-monomer polyethylene-like chains, each made out of six alternating units of propylene, acetylene and propylene organised in the following fashion: $\mathrm{H} - (-\mathrm{CH_2} - \mathrm{CH_2} - \mathrm{CH_2} - \mathrm{CH} = \mathrm{CH} - \mathrm{CH_2} - \mathrm{CH_2} - \mathrm{CH_2} -)_6 - \mathrm{H}$. The target structure was a polyethylene slab, periodic along x- and y-axes with a free surface along side z; the thickness was 50 Å and a target density as 0.3 g/cm^3. The configuration of the polymeric slab was obtained using a Monte Carlo based sampling of translational, rotational and conformational degrees of freedom based on the energies derived from the

PCFF forcefield [7] as implemented in the MedeA software package [4]. The density of the slab was fixed at approximately one-third of the experimental value to ensure the stability of the Monte Carlo simulation; the density was adjusted to match experimental later in the process.

The next step involved creating the CNT-polymer composite by introducing a CNT to the polymer bulk. Firstly, a void inside the polymer cell was created by introducing seven Lennard-Jones repulsive beads spaced equally between the centre of slab's free surface and a point inside the polymeric structure located at the midpoints of the periodic axis and 35 Å away from the surface into the slab in the non-periodic axis. The positions of the beads were fixed and they interacted with the polymer matrix via a Lennard-Jones repulsive potential creating a void that could accommodate a CNT. The strength of LJ repulsion was increased quasi-statically by changing the depth of the potential well from 0.1 kcal/mole to 4 Kcal/mole and the equilibrium distance from 1 Å to 8 Å over the course of ten iterations each involving a change of parameters followed by a geometry relaxation with the FIRE [1] algorithm with stopping criteria for the force below 10^{-10} eV/ Å or relative energy change below 10^{-10}. After ten iterations, the values were kept constant for 0.1 ns in an NVT simulation at 300 K to allow for local equilibration, after which the beads were removed from the matrix.

After the process was completed, a 30 Å long, $(10, 0)$ CNT fragment was placed inside the void; its position was chosen so that its longitudinal axis was aligned with the axis of the repulsive beads. The CNT C-C bond lengths were 1.42 Åand the terminated ends of the CNT were passivated with hydrogen atoms, the positions of which were optimised using the PCFF forcefield [7] in LAMMPS [6]. CNT functionalisation was later achieved by introducing three additional PE chains, identical to those used to construct the polymer bulk, which were attached to the CNT surface using amine, carbene or carboxyl functional groups or a [2 + 1] cycloaddition resulting in functionalisation density of one group per 100 CNT carbon atoms. The resulting interfaces are schematically shown in Figure 1 of the main text. Polymer chains grafted to the CNT surface were identical to those used to construct the polymer matrix and their position and orientation were selected to avoid particle overlap.

Afterwards, the system was equilibrated using an approach based on that of Ref. 3, which involves a series of temperature changes and compressions in the NPT ensemble. Firstly, the structure was compressed under the pressure of 0.5 GPa for 0.3 ns and then relaxed over the course of another 0.3 ns. The next step consisted of heating the sample to 800 K over 0.5 ns and subsequent cooling down to 300 K over the same period; this was followed by a compression-relaxation procedure like the one in the very beginning. After a more extended, 1 ns equilibration the process was completed.

Finally, the crosslinking of the polymer network was carried out with a procedure based on the comparison of distances between active carbon atoms in the acetylene molecules. When the separation between two atoms became smaller than a cutoff of 3.5 Å, a new bond between them was formed and the atom-types of participating atoms were changed to reflect their new cross-linked state; for generating realistic structures, it is important to note that only one atom in each acetylene unit may participate in cross-linking. This protocol was applied during a 0.5 ns simulation in an NVT ensemble at 800 K to generate a fully-connected polymer network.

The procedure described above yields a slab composed of 53 cross-linked polyethylene

chains reinforced with a 30 Å CNT functionalised with three groups, each forming a link between the nanotube and the matrix providing a atomistic model representation of a CNT-polymer composite material; an example structure is portrayed in Figure 2. of the main text. This protocol was repeated 40 times in order to produce an ensemble of ten different structures for each of the interface types.

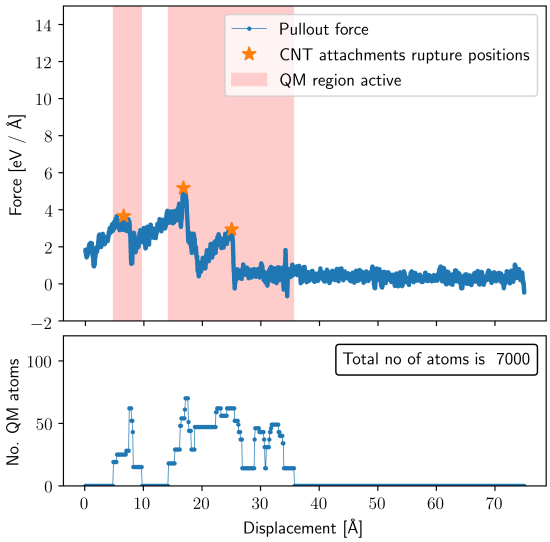

(a) Force-displacement curve for the system with a carbene group (CH_2) used as link.

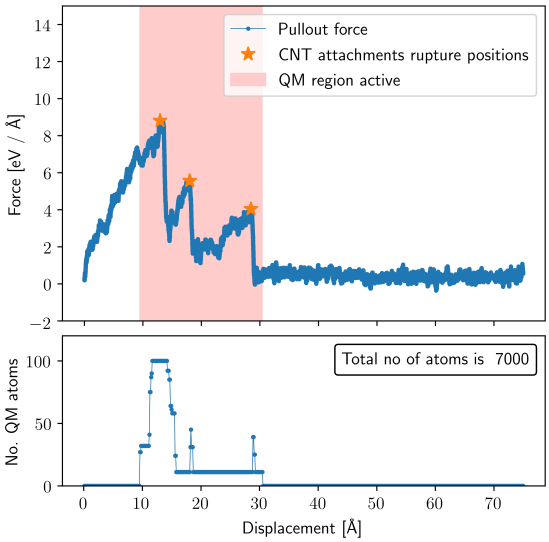

(b) Force-displacement curve for the system with a [2+1] carbene cycloaddition (CH) used as link.

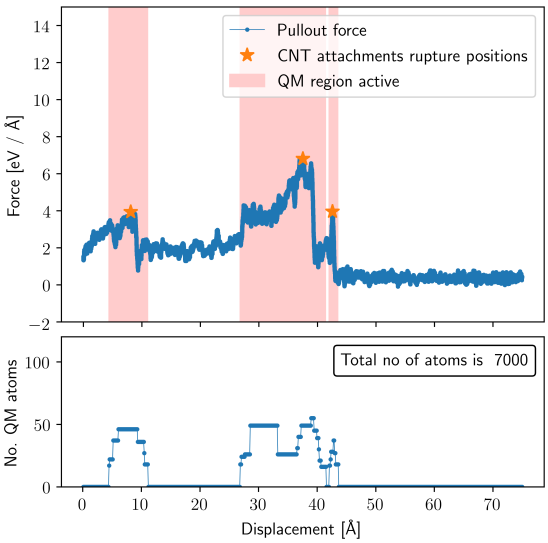

(c) Force-displacement curve for the system with an amine (NH) group used as link.

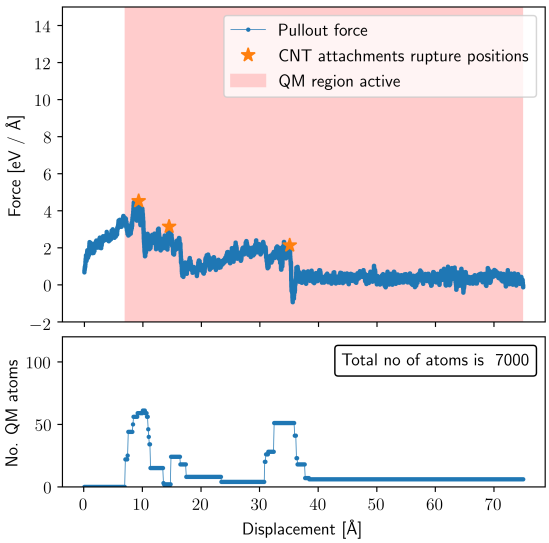

(d) Force-displacement curve for the system with a carboxyl group (COOH) used as link.

Figure S1: For each sub-figure, the top panel shows force vs displacement plot for a single representative simulation of the CH_2-functionalised system. The force peaks associated with bond-breaking events are highlighted (stars). Shaded areas show times when at least one atom was treated quantum mechanically. Bottom panel shows the total number of atoms marked as quantum mechanical at a given time. In the simulation presented in panel (d), the functional groups are not de-flagged following the detachment from the CNT as changes in bonding make it challenging for the classical force-field to provide an accurate description. Still, the number of QM atoms is greatly limited post-rupture as fewer than ten require a quantum description.

3 Critical strength of individual attachments

The times at which individual fracture events took place was found in an automated fashion by analysing the distance between two atoms in the functional group grafted to the CNT denoted as A_1 and A_2 in Figure S2. The bond between the two selected atoms is generally elongated when the attachment is transferring load between the polymer matrix and CNT and returns to equilibrium distance after a critical failure. A sudden change in the A_1-A_2 distance is used as an indicator of the time of the individual failure event.

The critical strength necessary to break an individual attachment is found by analysing the relation of the CNT pull-out force and the nanotube displacement, discussed in Section 2.1 of the main text. The peaks of the smoothed curve are located, and the values of maxima closest to the rupture location are chosen as the critical strengths. The plot of pull-out force alongside the appropriate interatomic distances for three CNT attachments for one of the simulations of a system with CH_2 functional attachments is shown in Figure S3.

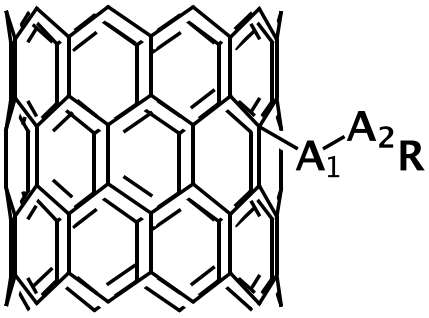

Figure S2: Polymer attachment point with two atoms used for attachment monitoring annotated as A_1 and A_2.

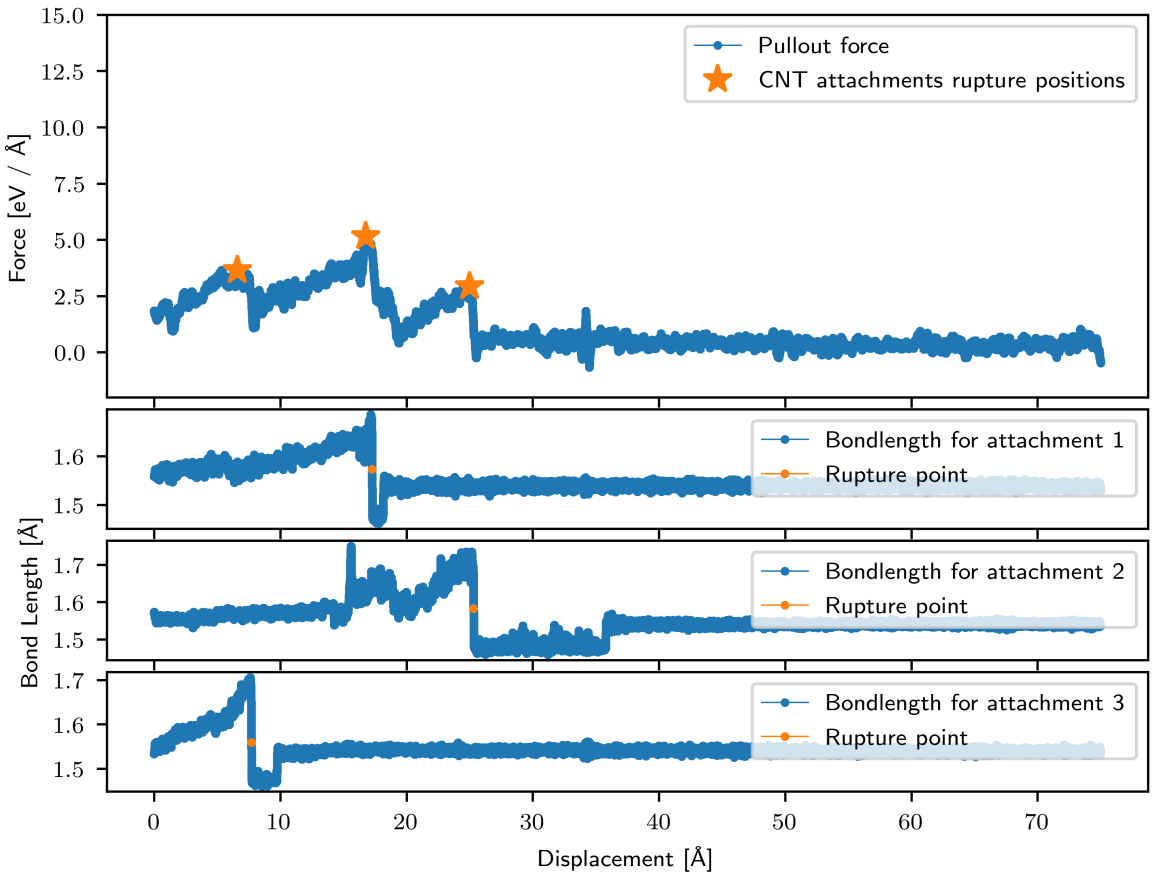

Figure S3: Top panel: Force vs displacement plots for a selected simulation for the CH_2 system. Lower panels: plots of selected bond-length used to monitor all three individual attachment status.

4 Temperature dependence

As mentioned in Section 2 of the main text, the pull-out simulations were carried out at a temperature of 100 K instead of room temperature of 300 K in order to reduce thermal variations of atoms and make QM flagging more consistent, limiting unphysical fluctuations in the set of flagged atoms. The effect of changing the temperature from 100 K to 300 K was quantified by conducting two series each of ten simulations exploring pull-out of a CNT functionalised with carbene groups at temperatures of 100 K and 300 K; all simulations were performed as discussed in Section 2.1 of the main text. The results of the critical force on the constrained CNT atoms, critical strength of individual attachments and the fracture energy of the interface are shown in Figure S4, Figure S5 and Figure S6, respectively. The discrepancy of results between tests performed at different temperatures is small, and as a result, simulations performed at 100 K were considered to be a good approximation of the behaviour at room temperature.

We believe that bond-breaking occurs as a result of work done by the pull-out force rather than thermal fluctuations overcoming energy barriers. In our simulations, interfacial failure

was caused by the detachment of carbene, azide of carboxyl groups from the CNT surface, or rupture of carbon-carbon bonds inside the polymer chain. The adsorption energies for CH_3, NH_2 and COOH molecules attached to the CNT are approximately 1.0, 1.0 and 1.6 eV respectively [5] while the dissociation energy for a C-C bond in ethylene is approximately 3.9 eV [2]. This is significantly higher than the thermal fluctuations energy at 300K or 100K which account to 2.5×10^{-2} and 8.6×10^{-3} eV respectively which, we believe, is the main reason for the negligible effect of temperature change on ISS measurements.

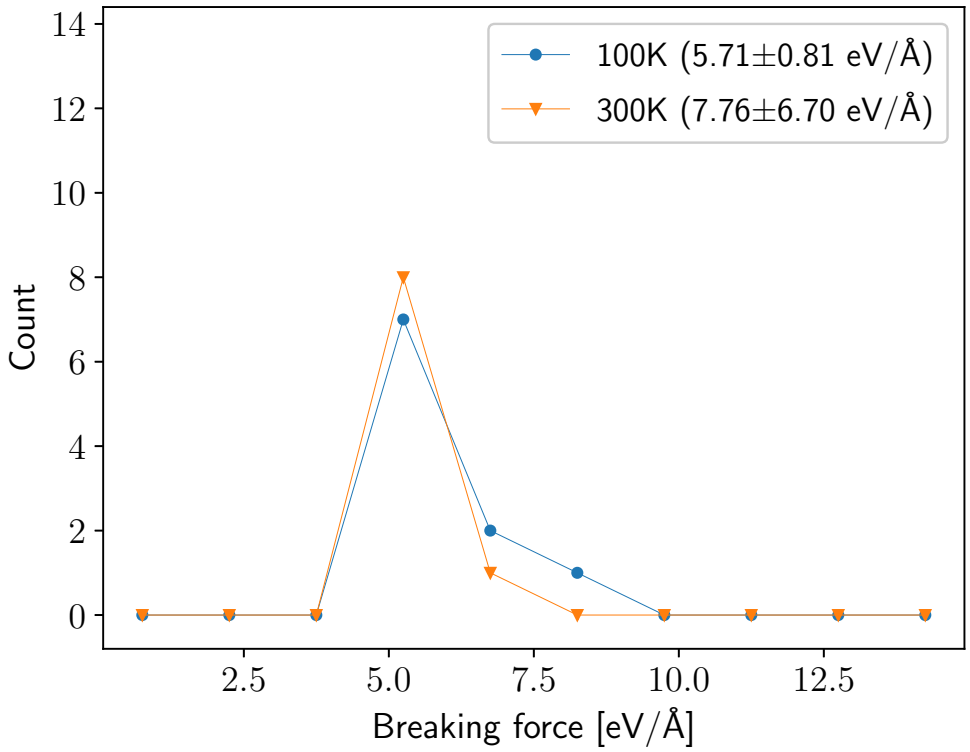

Figure S4: Distribution of critical force on the constrained CNT atoms for the ch interface at two temperatures. The bins used in the histogram have the width of 1.5 eV/Å with the leftmost edge of the first bin located at 0; the markers are placed at the midpoint of each bin.

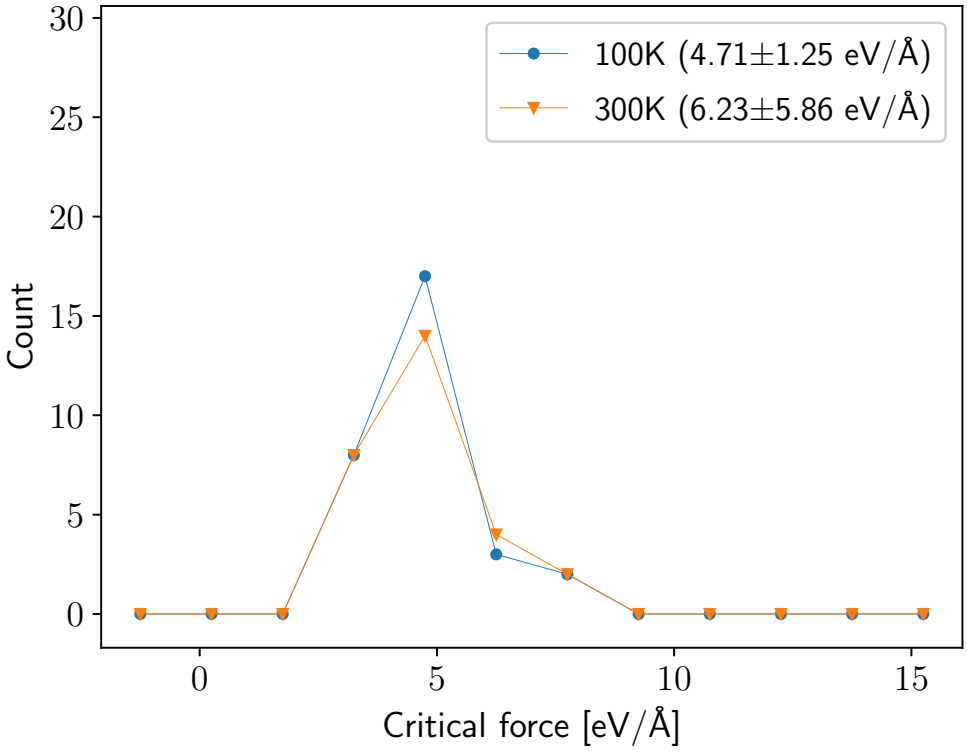

Figure S5: Distribution of critical strength of individual attachments for for the ch interface at two temperatures. The bins used in the histogram have the width of 1.5 eV/Å with the leftmost edge of the first bin located at 0; the markers are placed at the midpoint of each bin.

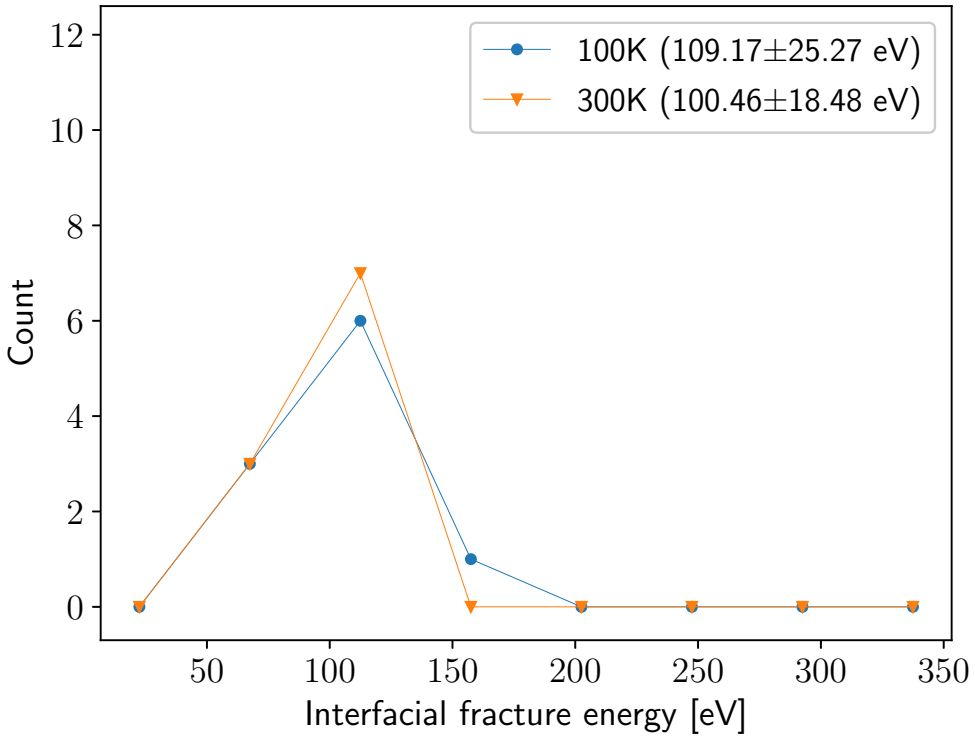

Figure S6: Distribution of fracture energy for for the ch interface at two temperatures. The bins used in the histogram have the width of 45 eV with the leftmost edge of the first bin located at 0; the markers are placed at the midpoint of each bin.

5 Comparison between DFTB and full DFT

We have investigated the disparity between DFTB and full DFT by comparing atomic forces obtained using the classical forcefield used in this work, the DFTB model and full DFT. We have selected a single CH_2 functionalised CNT pull-out simulation and picked 30 snapshots of the atomic configuration covering 5 ps around a single functional group rupture event. For each of the snapshots, the QM cluster from the original simulation (constructed as discussed in the main text) was used to compute forces on flagged atoms (flagging taken from the original simulation) using all three methods. Finally, DFTB and classical forces were compared against the full DFT results as presented in Figure S7. The findings show that DFTB is in good agreement with the full DFT description of the atomic forces and is much more accurate than the classical forcefield. As a result, we believe that DFTB-based QM/MM pull-out simulations can be reliably used to reach the conclusions presented in the main text.

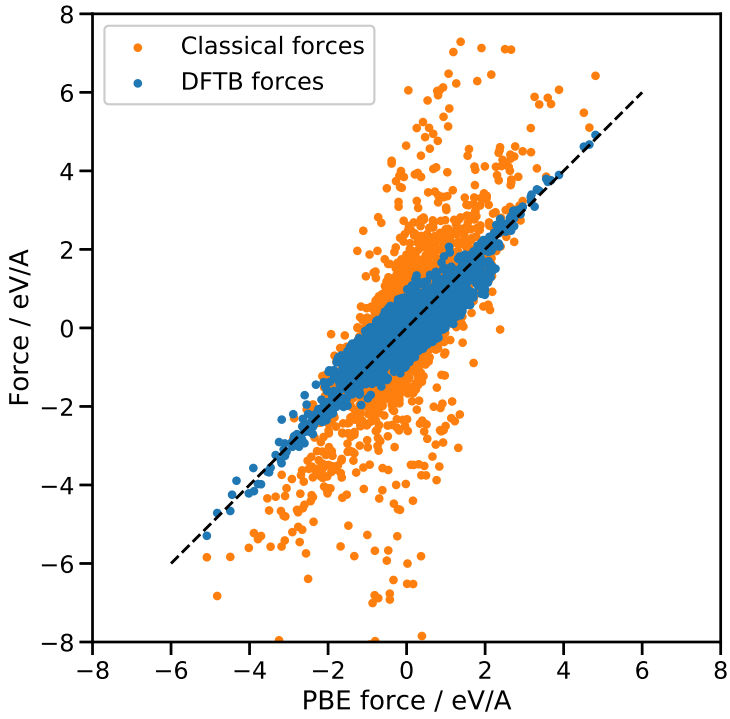

Figure S7: Comparison of atomic forces computed using DFTB, DFT and the classical forcefield. Systems used for comparison were constructed by selecting 30 atomic snapshots from a CH_2 pull-out simulation, covering 5 ps around a single functional group rupture event. For each of the snapshots, the QM cluster from the original simulation was used to compute forces on flagged atoms using all three methods. Each point is located at coordinates dictated by the atomic force from a DFT simulation (with the PBE exchange and correlation functional) on the horizontal axis and atomic force from DFTB (blue) and the classical forcefield (orange) the vertical axis.

The DFT calculations of the forces on 30 QM clusters extracted from the QM/MM dynamics, each containing 250 atoms, were carried out with the CASTEP code using ultrasoft pseudopotentials and a plane wave basis set with a 400 eV cutoff energy. The QM regions were surrounded by 8 Å of vacuum; a single k-point at Γ was thus used to sample the Brillouin zone. Occupancies were modelled with Gaussian smearing with a width of 0.2 eV. The PBE paramaterisation of the generalised gradient approximation to the exchange correlation functional was used, along with a spin-polarised treatment of the wavefunctions. The convergence tolerance for the self-consistent field minimisation was 10^{-5} eV/atom. The DFTB and classical forcefield calculations were performed following the description in the main text. For comparison with the QM/MM case, note that each DFT calculation took around 3 hours on 64 processors while the same simulation with DFTB took approximately 5 seconds on 28 proceessors.

References

[1] E. Bitzek, P. Koskinen, F. Gähler, M. Moseler, and P. Gumbsch. Structural relaxation made simple. *Physical Review Letters*, 97(17):1–4, 2006.

[2] S. J. Blanksby and G. B. Ellison. Bond Dissociation Energies of Organic Molecules. *Accounts of Chemical Research*, 36(4):255–263, 2003.

[3] E. Kucukpinar and P. Doruker. Molecular simulations of gas transport in nitrile rubber and styrene butadiene rubber. *Polymer*, 47(22):7835–7845, 2006.

[4] Materials Design, Inc., Angel Fire, NM, USA. Medea.

[5] K. Z. Milowska and J. A. Majewski. Functionalization of carbon nanotubes with -CHn, -NHnfragments, -COOH and -OH groups. *Journal of Chemical Physics*, 138(19):194704, may 2013.

[6] S. Plimpton. Fast Parallel Algorithms for Short âĂŞ Range Molecular Dynamics. *Journal of Computational Physics*, 117(June 1994):1–19, 1995.

[7] H. Sun, S. J. Mumby, J. R. Maple, and A. T. Hagler. An ab Initio CFF93 All-Atom Force Field for Polycarbonates. *Journal of the American Chemical Society*, 116(7):2978–2987, 1994.

[8] J. Wang, R. M. Wolf, J. W. Caldwell, P. A. Kollman, and D. A. Case. Development and testing of a general Amber force field. *Journal of Computational Chemistry*, 25(9):1157–1174, jul 2004.

[9] L. Zhechkov, T. Heine, S. Patchkovskii, G. Seifert, and H. A. Duarte. An efficient a posteriori treatment for dispersion interaction in density-functional-based tight binding. *Journal of Chemical Theory and Computation*, 1(5):841–847, 2005.